Base-pairing of uracil and 2,6-diaminopurine: from cocrystals to photoreactivity

Tomislav Stolar,*,† Ben K. D. Pearce,‡ Martin Etter,¶ Khai-Nghi Truong,§ Andraž Krajnc,‖ Gregor Mali,‖ Barbara Rossi,⊥ Krešimir Molčanov,† Ivor Lončarić,† Ernest Meštrović,*,# Krunoslav Užarević,*,† and Luca Grisanti*,†,@

†*Ruđer Bošković Institute, 10000 Zagreb, Croatia*

‡*Johns Hopkins University, Baltimore, MD 21218, USA*

¶*Deutsches Elektronen-Synchrotron (DESY), 22607 Hamburg, Germany*

§*Rigaku Europe SE, 63263 Neu-Isenburg, Germany*

‖*National Institute of Chemistry, 1000 Ljubljana, Slovenia*

⊥*Elettra Sincrotrone Trieste, 34149 Trieste, Italy*

#*Faculty of Chemical Engineering and Technology, University of Zagreb, 10000 Zagreb, Croatia*

@*National Research Council - Materials Foundry Institute (CNR-IOM) c/o SISSA (International School for Advanced Studies), 34136 Trieste, Italy*

E-mail: tomislav.stolar@gmail.com; emestrov@fkit.hr; krunoslav.uzarevic@irb.hr; luca.grisanti@irb.hr

Abstract

The information molecule of the first life on Earth is presumably ribonucleic acid (RNA). RNA is a polymer built out of four canonical nucleobases: adenine (A), uracil (U), guanine (G), and cytosine (C). However, it remains unclear how canonical nucleobases got selected from the hundreds available in nature. Here, we show that the

non-canonical nucleobase 2,6-diaminopurine (D) base pairs with U in water and the solid state without the need to be attached to the ribose-phosphate backbone. Depending on the temperature and water availability in the system, D and U assemble in thermodynamically stable hydrated and anhydrated D-U base-paired cocrystals. Structural studies show that the water molecules contribute favorably to the stabilization energies in D-U cocrystal hydrate due to the role of water in forming inter-layer hydrogen bonds. In the anhydrate cocrystal form, D and U molecules exhibit advantageous homomeric stacking interactions and hydrogen bonding. Under UV irradiation, an aqueous solution of D-U base-pair undergoes photochemical degradation, while a pure aqueous solution of U does not, thus demonstrating that base-pairing alters the photostability of U. To understand this decreased photostability of U, we model the main channel for U photodestruction, i.e., covalent photodimerization. Our simulations suggest that D may trigger the U photodimerization because of its ability to form hydrogen bonds with π-stacking dimers of U. Our results indicate that complementary base-pairing of D and U in prebiotic surface environments may have played a role in chemical evolution. In a broader context, supramolecular interactions between small biological building blocks may offer new insights into the origin of life.

Introduction

Canonical nucleobases are attached to the sugar-phosphate backbone in nucleic acids and act as molecular recognition units. Their complementary base-pairing is central to the transfer of genetic information.[1] Moreover, base-pairing of free canonical nucleobases (without being attached to the sugar-phosphate backbone) might have been a starting point for the origin of nucleic acids.[2] However, it has been known for almost 60 years that there is no molecular recognition and complementary base-pairing of free canonical nucleobases in water.[3,4] Instead, they form energetically favored stacking structures and hydrogen bonds with water molecules.[5] We recently showed that base-pairing of free canonical nucleobases does

not occur even in the solid-state reaction environment devoid of water.[6] This inability of free canonical nucleobases to spontaneously form Watson-Crick base pairs is known as a "base-pairing paradox",[7] making it unclear how the chemical selection of nucleobases occurred from a larger pool of similar molecules likely available on the prebiotic Earth.[8–12] On one hand, it has been proposed that RNA is a product of evolution.[13] Under this assumption, proto-RNA forms could have been constituted by different components, including nucleobases, whose chemical bonding was easier under prebiotic conditions.[12,14,15] An alternative scenario is that RNA formed *de novo* on the prebiotic Earth and bypassed chemical selection on the level of nucleobases.[16] For example, prebiotic syntheses of canonical nucleosides and nucleotides have been reported and include the formation of the glycosidic bond between more reactive substances and subsequent building of nucleobases on the sugars.[17,18] Nevertheless, the base-pairing of free canonical or non-canonical nucleobases may affect their chemical properties and remains largely unexplored in the literature. Hence, it serves as a motivation for this work.

Non-canonical nucleobases are intriguing, as they would have been present during chemical evolution, and some even play roles in life processes today. For example, D is present in meteorites alongside U, and its extraterrestrial origin is confirmed.[19,20] When incorporated into DNA, D repairs UV-induced lesions.[21] Nucleoside and nucleotide analogs of D are also products of selective prebiotic syntheses.[18,22] Remarkably, D is even present in contemporary biology as it completely substitutes A in the genomes of a wide array of siphoviruses.[23–27] Looking at the molecular level, D contains an additional amino group in the 2 position compared to A and can form up to three intermolecular hydrogen bonds with U (Figures 1a and 1b). On the other hand, Watson-Crick hydrogen bonding between A and U by two intermolecular hydrogen bonds occurs when attached to the sugar-phosphate backbone but is absent on the level of free nucleobases. If available under prebiotic conditions, thermodynamically more favorable D-U base-pairing is important in understanding the chemical evolution of these two nucleobases. For example, the complementary supramolecular assembly of D

and U could affect their photostability under UV light.[28] Importantly, solar radiation was likely the primary source of energy available on early Earth and a key factor for chemical selection.[29]

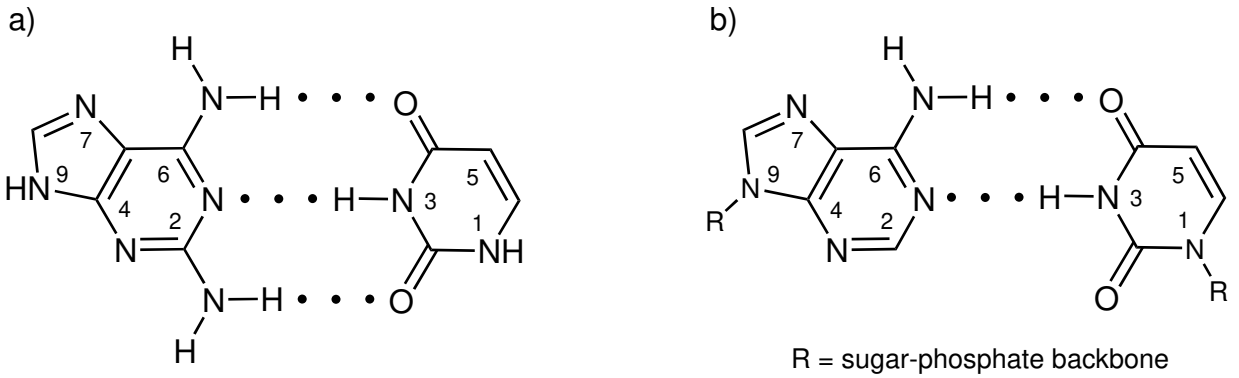

Figure 1: a) Molecular structures of D (left) and U (right) with highlighted hydrogen bonding complementarity. This base pair has the potential to form up to three intermolecular hydrogen bonds. b) Molecular structures of A (left) and U (right) with Watson-Crick base-pairing motif by two intermolecular hydrogen bonds. This base-pairing occurs in nucleic acids but does not occur on the level of free nucleobases in the absence of a sugar-phosphate backbone.

In this work, we combine several state-of-the-art experimental and computational techniques to investigate the interaction of D and U, the formation of their assemblies in different aggregate states (crystal, liquid, and gas), and discuss the impact on photochemistry concerning early Earth environments. We reveal the self-assembly of D-U cocrystal hydrate (**D-U hyd**) and anhydrate (**D-U anhyd**) under prebiotic reaction conditions of different water availability (bulk water, stoichiometric water, water vapor, and dry state) and temperatures (low and elevated). We monitor the formation of **D-U hyd** and its wet/dry cycling to **D-U anhyd** by *in situ* synchrotron powder X-ray diffraction (PXRD). We elucidate the crystal structure of **D-U hyd** from single crystal X-ray diffraction (SCXRD) data and **D-U anhyd** from 3D electron diffraction (ED) data to study the crystal packing. We estimate favorable formation and stabilization energies of D-U base-paired cocrystals by periodic density functional theory (DFT) computation and reveal the formation of Watson-Crick dimers as a driving force for their assembly. To place D-U base-paired cocrystals in the prebiotic context,

we study the photostability of its aqueous solution under UV light by *in situ* UV resonance Raman (UVRR) measurements. The latter shows that it is significantly less photostable than the aqueous solution of pure U. This is surprising since U, and more generally canonical nucleobases, are typically very stable when irradiated by UV light in their free forms, including in aqueous solutions.[28] This behavior is associated with a very short excited-state lifetime at the order of picoseconds. In the case of free U, such rapid radiationless deactivation from $\pi\pi^*$ state involves a conical intersection (CI) along a coordinate corresponding to the twist around the double C5C6 bonds.[30,31] However, as we show in this work, the situation differs when non-covalent interactions between complementary nucleobases, such as D and U, are in place.[32] Furthermore, we perform quantum-chemical and DFT simulations to show that D-U hydrogen bonding may promote photoreaction to form cyclobutane pyrimidine dimers (CPDs) of U. Thus, serving as a possible pathway for the photochemical degradation of U that needs at least two U nucleobases to be in proximity to be effective.

Experimental section

Materials and characterization. Uracil (U) and 2,6-diaminopurine (D) were purchased from Carbosynth. Grinding experiments were conducted in 14 mL poly(methyl methacrylate) (PMMA) containers using InSolido Technologies vibratory ball mill. Two 1.4 g stainless steel balls (7 mm in diameter) were used as milling media and the reactions were conducted at a 30 Hz frequency. In grinding reactions with H_2O, 20 μL of H_2O was added to the overall 200 mg of the reaction mixture (1.5:1 ratio of H_2O to D and U). Grinding under low-temperature conditions was performed using liquid nitrogen. PMMA jars containing the reaction mixture were immersed in liquid nitrogen before mounting on the mill and liquid nitrogen was poured continuously over the jars during 30 min of ball milling. Slurry reactions were performed by stirring an aqueous suspension of D and U (equimolar amounts of D and U, overall mass of the reaction mixture 100 mg) in 3 mL of distilled H_2O at room

temperature in a 10 mL round bottom flask. Aging reactions were conducted by placing a plastic tube containing a solid sample in a glass bottle whose bottom was filled with distilled H_2O. The aging setup was a closed system and the glass bottle was closed with a cap. Ex situ PXRD data were collected on Panalytical Aeris tabletop X-ray diffractometer, with CuK_α radiation (40 kV, 7.5 mA) in Bragg-Brentano geometry, with the sample mounted on a zero background silicon plate. TGA and DSC experiments were performed by Simultaneous thermal analyzer (STA) 6000 (PerkinElmer, Inc.) in platinum crucibles at 5 °C min^{-1} heating rate under nitrogen gas purging at a flow of 20 mL min^{-1}. Rietveld refinement[33] was performed in TOPAS.[34]

***In situ* synchrotron PXRD monitoring of grinding and wet/dry cycling**. *In situ* monitoring of grinding D and U with H_2O was performed at the P02.1 beamline at PETRA III, DESY (Hamburg, Germany). 20 μL of H_2O was added to the overall 200 mg of the equimolar D and U reaction mixture (1.5:1 ratio of H_2O to D and U). The X-ray beam ($\lambda = 0.20741$ Å) was set to pass through the bottom of the PMMA reaction vessel. Exposure time was set to 10 s. Diffraction data were collected on a Perkin Elmer XRD1621 flat-panel detector positioned 1595 mm from the sample, which consisted of an amorphous Si sensor equipped with a CsI scintillator (pixel number: 2048 x 2048, pixel size: 200x200 µm**²**). To obtain the classic one-dimensional PXRD pattern, the two-dimensional diffraction images were integrated with the DAWN Science package. Variable-temperature PXRD for wet/dry cycling of **D-U hyd** was performed at P02.1 beamline at PETRA III, DESY (Hamburg, Germany). A capillary of 0.5 mm width was filled with ca. 5 mg of **D-U hyd** sample and was heated using Oxford Cryostream system (operating in 100-500 K temperature range). The distance between the sample and the detector was 2010 mm. X-rays of 0.20741 Å wavelength were used, and X-ray diffraction patterns were collected on a spinning capillary. The sample was thermally equilibrated at 300 K and was heated using a 5 K/min ramp rate. X-ray diffraction patterns were collected in 10 K steps. After reaching the desired temperature set-point, the sample was thermally equilibrated, and X-ray diffraction pattern

was collected. The exposure time for each collected diffraction pattern was 60 s for the dark image plus 60 s for the real image. To obtain 2D plots for *in situ* synchrotron PXRD monitoring, data were processed in MATLAB.

Single-crystal X-ray diffraction. To obtain single crystals of **D-U hyd**, 15 mg of a dry ground equimolar mixture of D and U was dissolved in 5 mL of methanol. Single-crystals were grown after solvent evaporation at room temperature. Single crystal measurements were performed on an Oxford Diffraction Xcalibur Nova R (microfocus Cu tube) equipped with an Oxford Instruments CryoJet liquid nitrogen cooling device. Program package CrysAlis^{PRO} [35] was used for data reduction and numerical absorption correction. The structures was solved using SHELXS97 and refined with SHELXL-2017.[36] The model was refined using the full-matrix least-squares refinement; all non-hydrogen atoms were refined anisotropically. Hydrogen atoms were located in a difference Fourier map and refined as a mixture of free-restrained and riding entities. The co-crystallized water molecule (O3) is disordered over two positions (designated as A and B) with respective occupancies of 63% and 37%. Molecular geometry calculations were performed by PLATON[37] and molecular graphics were prepared using ORTEP-3,[38] and Mercury.[39] Crystallographic and refinement data for **D-U hyd** is shown in Figure S15. The structure has been deposited in the Cambridge Crystallographic Data Centre (CCDC) as no. 2059340.

3D electron diffraction. ED measurements for **D-U anhyd** were collected using the Rigaku XtaLAB Synergy-ED, equipped with a Rigaku HyPix-ED detector optimized for operation in the continuous rotation 3D-ED experimental setup.[40] Data acquisition was performed at ambient temperature under high vacuum with an electron wavelength of 0.0251 Å. The instrument was operated and the diffraction data were processed in the program CrysAlis^{PRO}.[41] A multi-scan absorption correction was performed using spherical harmonics implemented in SCALE3 ABSPACK scaling algorithm in CrysAlis^{PRO}. The structure was solved using ShelXT,[36] and subsequently, refined with kinematical approximation using ShelXL[42] in the crystallographic program suite Olex2.[43,44] By merging data of three indi-

vidual grains/datasets, completeness of 96.2% up to a resolution of 0.80 Å was achieved. Non-hydrogen atoms were assigned anisotropic displacement parameters unless stated otherwise. The hydrogen atoms bonded to nitrogen atoms were located from Fourier difference maps. Other hydrogen atoms were placed in idealized positions and included as riding. Isotropic displacement parameters for all hydrogen atoms were constrained to multiples of the equivalent displacement parameters of their parent atoms with $U_{iso}(\mathrm{H}) = 1.2\ U_{eq}$(parent atom). Enhanced rigid bond restraints[45] with standard uncertainties of 0.001 Å^2 was applied. The experimental and refinement details are given in Figure S16. The crystal structure of **D-U anhyd** has been deposited in CCDC as no. 2247776.

Periodic DFT simulations. Periodic plane-wave DFT calculations were performed with Quantum Espresso[46,47] using GBRV pseudopotentials[48] and vdW-DF-cx[49,50] exchange-correlation functional that is well suited for this type of systems.[51–54] The plane-wave basis set cutoff is 600 eV, and the first Brillouin zone is sampled by the Monkhorst–Pack k-point mesh with a density of 5 Å. Coordinates from experimental XRD were relaxed according to BFGS algorithm, first by keeping cell parameters equal to experimental, and then further relaxed allowing for combined unit cell and positions relaxations. From these two DFT calculations (0 K) minimization, we respectively obtained *rigid-cell formation energy*:

$$\begin{aligned} E^{\mathrm{form}}_{\mathrm{rigid\ cell}}(\text{D-U hyd}) =& E(\text{D-U hyd})^{\text{exp. cell}} - [E(\text{D hyd})^{\text{exp. cell}} + E(\mathrm{U})^{\text{exp. cell}}] \\ E^{\mathrm{form}}_{\mathrm{rigid\ cell}}(\text{D-U anhyd}) =& E(\text{D-U anhyd})^{\text{exp. cell}} \\ & - [E(\text{D hyd})^{\text{exp. cell}} + E(\mathrm{U})^{\text{exp. cell}} - E(\mathrm{H_2O\ Ih\ ice})^{\text{exp. cell}}] \end{aligned}$$

and *full formation energy*:

$$\begin{aligned} E^{\mathrm{form}}_{\mathrm{full}}(\text{D-U hyd}) =& E(\text{D-U hyd})^{\text{relaxed cell}} - [E(\text{D hyd})^{\text{relaxed cell}} + E(\mathrm{U})^{\text{relaxed cell}}] \\ E^{\mathrm{form}}_{\mathrm{full}}(\text{D-U anhyd}) =& E(\text{D-U anhyd})^{\text{relaxed cell}} \\ & - [E(\text{D hyd})^{\text{relaxed cell}} + E(\mathrm{U})^{\text{relaxed cell}} - E(\mathrm{H_2O\ Ih\ ice})^{\text{relaxed cell}}] \end{aligned}$$

where each energy term embeds factors to compare the different unit-cell stoichiometries. These results are reported in Table S1. For in-vacuum complexes and interaction energy V_{AB} (Table S2), results were obtained using periodic DFT by relaxing clusters obtained from crystal placed in a large unit cell (box size of 70. a_0), so to minimize interaction between periodic images. The usage of planewave-DFT avoid any superposition errors in estimating the interaction energies in molecular clusters. Periodic DFT simulations were run at the high-performing computing cluster of the Division of Theoretical Physics of the Ruđer Bošković Institute, Zagreb, Croatia.

UV resonance Raman spectroscopy. Multi-wavelength UVRR spectra have been collected at the BL10.2-IUVS beamline of Elettra Sincrotrone Trieste by exploiting the experimental setup described in detail in Ref.[55] Different excitation wavelengths in the deep UV range (220-270 nm) were employed. These excitation conditions were chosen to obtain suitable resonance Raman signals for the examined samples and, at the same time, the best features in terms of the spectral resolution and signal-to-noise ratio in the whole concentration range considered. In particular, the reported quantitative information specifically refers to the UVRR spectra acquired using 266 nm as excitation wavelength. The Raman signal was collected in back-scattered geometry using a single pass of a Czerny-Turner spectrometer (Trivista 557, Princeton Instruments, 750 mm focal length) and detected with a UV-optimized CCD camera. The spectral resolution was set at 1.2 cm^{-1}/pixel. The calibration of the spectrometer was standardized using cyclohexane (spectroscopic grade, Sigma-Aldrich). The power of the beam on the sample was measured to be 0.3-0.4 mW with a spot area of about 1 mm^2. Solid samples (D, U, and **D-U hyd**) were dissolved in pure water. Such freshly prepared solutions were placed in suitable suprasil-quartz cuvettes with an optical path of 10 mm. Atmosphere in cuvette was made inert by nitrogen flow, and then measured under a magnetic stirrer. During the Raman measurements, the temperature of the solutions was controlled using a sample holder equipped with a thermal bath coupled to a resistive heating system to keep the temperature of the sample at a fixed value with the

stability of ±0.1 °C. The collected UVRR spectra were subtracted from a 2-order polynomial baseline and the cosmic rays were removed. We have assessed the intensity of the bands of interest through an integration algorithm applied to the wavenumber regions of interest.

Quantum-chemical and DFT simulations in-vacuum. Ground and excited state 2D potential energy surfaces for UU and D-UU dimerization were calculated using the *Gaussian09* package[56] on the Graham cluster operated by Compute Canada. Energies were calculated using the wB97XD functional[57] and 6-31G* basis set.[58] Ground state optimizations involved freezing two carbon-carbon bonds between U and U (using the opt=modredundant keyword) from 1.5 to 4.0 Å. Scans from 1.5 to 2.6 Å were performed with a precision of 0.1 Å, and scans from 2.6 to 4.0 Å were performed with a precision of 0.2 Å. Both unrelaxed and relaxed scans were also performed for the first excited state using TDDFT starting from the ground state geometries. In addition, at the same level of theory, a full ground state minimization was run for each of the basins identified in the PESs for UU and D:UU, followed by TDDFT evaluation of excitation energies and first excited state relaxations. After a proper evaluation of the active spaces, CI optimizations through *opt=conical* via CASSCF(4,4) for UU and CASSCF(6,6) for DU:U and 6-31G* basis set using *Gaussian16* package[59] were successfully performed. These final CASSCF calculations were run at the Isabella cluster in Zagreb, Croatia.

Results and discussions

Stirring an aqueous suspension of D and U for six days at room temperature resulted in a product primarily composed of D-U cocrystal hydrate (**D-U hyd**, Figures S1 and S2). Dry grinding of D and U for 2 h resulted in a product with an amorphous PXRD pattern (Figure S1) which, upon aging[60] in H_2O vapor for seven days at room temperature, transformed to **D-U hyd** (Figure S1). The input of mechanical energy, considered an important energy source for prebiotic chemistry,[61–65] is not a prerequisite for **D-U hyd** formation in moisture. Gentle

homogenization of D and U with the spatula and aging in H_2O vapor at room temperature also resulted in the formation of **D-U hyd** (Figures S1 and S3). We monitored the grinding of D and U with a stoichiometric amount of H_2O by *in situ* synchrotron PXRD (Figure 2a). It showed that **D-U hyd** started to form within the first minute of grinding, and the reaction mixture was phase pure by 30 min (Figures S4 and S5). Additionally, we studied the base-pairing of D and U under low-temperature conditions (Figures S6-S8). After 30 min of grinding D and U with a stoichiometric amount of H_2O at ca. 80 K, PXRD analysis confirmed the formation of **D-U hyd** (Figure S1).

We also performed wet-dry cycling[66] in a sealed glass capillary and monitored it by *in situ* synchrotron PXRD (Figure 2b). **D-U hyd** was thermally stable until 410 K, when it started transforming into different crystalline phases (Figure S9). Rietveld analysis showed that after heating to 490 K (Figure S10), the solid sample was composed of **D-U anhyd**, D hydrate,[67] and D anhydrate.[68] Similarly, heating **D-U hyd** to 530 K in an open container (Figure S11) resulted in a solid sample composed of **D-U hyd**, **D-U anhyd**, D hydrate, and D anhydrate (Figures S12). The latter was consistent with the ^{1}H-^{13}C cross-polarization magic-angle spinning nuclear magnetic resonance spectra which showed that the sample was not phase pure (Figure S13).

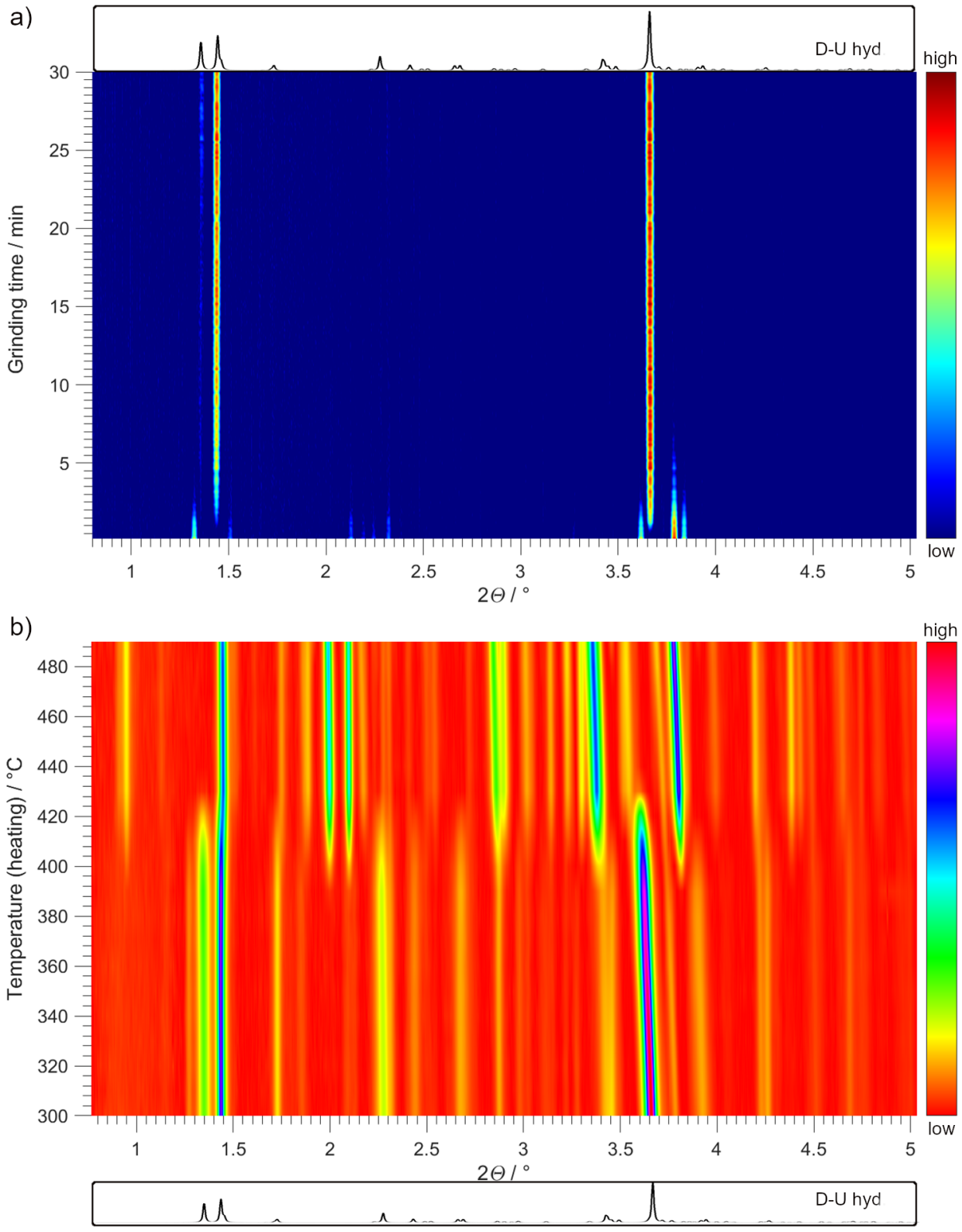

Figure 2: a) *In situ* monitoring of grinding 200 mg of an equimolar amount of D and U with 20 μL of H_2O by synchrotron PXRD (λ = 0.20741 Å). A simulated PXRD pattern of **D-U hyd** is given in a box at the top. b) *In situ* monitoring of heating **D-U hyd** in a sealed glass capillary by synchrotron PXRD (λ = 0.20741 Å). A simulated PXRD pattern of **D-U hyd** is given in a box at the bottom. Note: some Bragg reflections are shifting towards lower 2Θ values during heating due to the expansion of the unit cell.

We also tested if D-U base-pairing occurs in the presence of A. We employed different reaction conditions and demonstrated that D-U base-pairing is selective and occurs with A in the reaction mixture (Figure S14). Furthermore, the reaction conditions we tested for base-pairing of equimolar mixtures of D and U include different scenarios of prebiotic water availability,[69,70] ranging from bulk water to dry conditions. One such scenario on an early Earth involves wet/dry cycling in hydrothermal pools,[66,71,72] which are considered to be important for the origin of life. Moreover, some of the reaction conditions that we used might be compatible with meteorite post-accretion events such as aqueous alteration[73] and hydrous metamorphism.[74] This is relevant since both D and U have been detected in meteorites,[19,20] and the chemical evolution of organic inventory under extraterrestrial conditions is of increasing interest.[75]

To understand the intermolecular interactions of D and U in the solid state, we solved the crystal structures of **D-U hyd** from SCXRD data (Figure S15) and **D-U anhyd** from 3D ED data (Figure S16 and S17). **D-U hyd** is a 1:1 stoichiometry cocrystal channel hydrate whose asymmetric unit comprises D and U molecules assembled by three intermolecular hydrogen bonds and disordered water molecule (Figure S18a). In the crystal, D and U molecules form hydrogen-bonded layers with D-U and D-D hydrogen bonding (Figure 3a). Interestingly, each D molecule forms eight hydrogen bonds, thus involving all possible hydrogen bonding donors and acceptors. Besides filling structural voids and lying in the channels (Figure S18b), the disordered water molecules act as bridging elements connecting adjacent layers through hydrogen bonding (Figure S18c). On the other hand, **D-U anhyd** is a 1:2 stoichiometry cocrystal anhydrate whose asymmetric unit contains two molecules of U and one molecule of D (Figure S19a). Besides D-U interactions, hydrogen-bonded layers also exhibit homomeric U-U hydrogen bonding interactions (Figure 3b). Similarly, each D molecule forms eight hydrogen bonds, involving all possible hydrogen bonding donors and acceptors. Between the layers, this crystal also exhibits homomeric parallel displaced π-π stacking interactions distanced at 3.7 Å (Figure S19b).

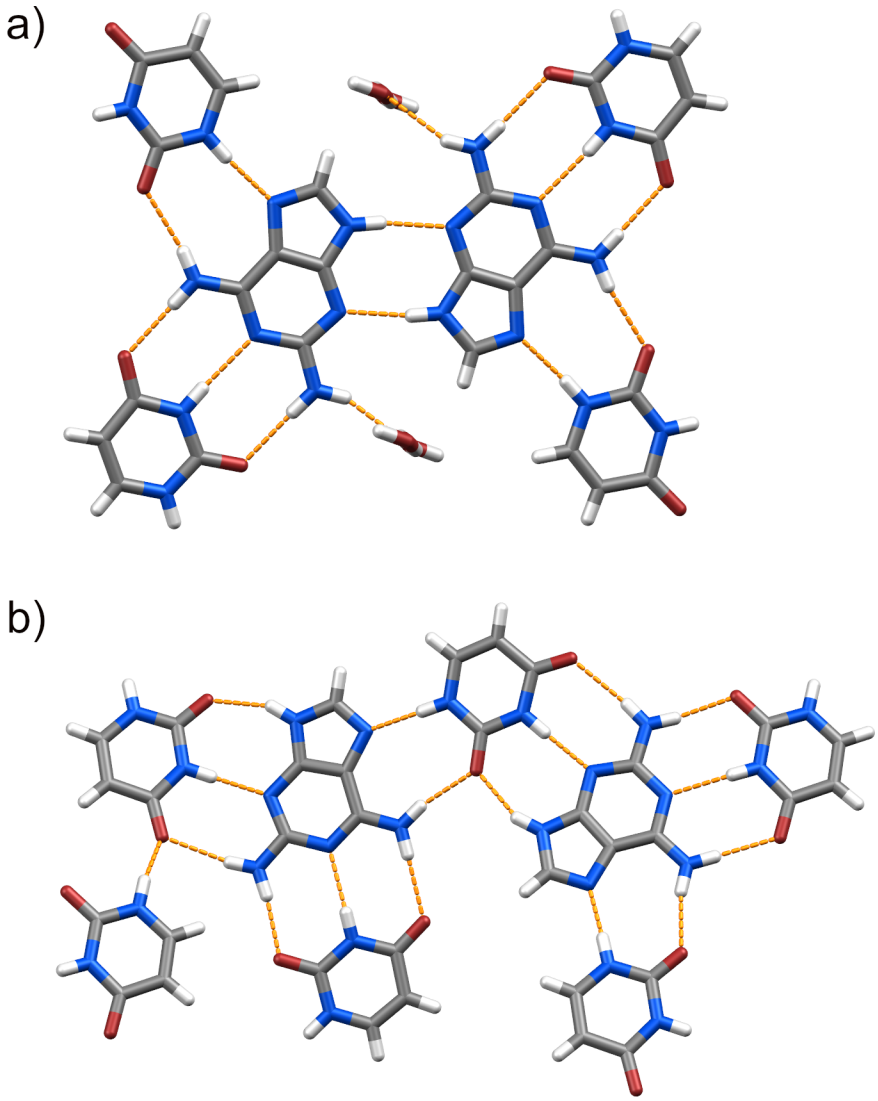

Figure 3: a) Hydrogen-bonded layers in **D-U hyd** exhibit D-U and D-D hydrogen bonding. b) Hydrogen-bonded layers in **D-U anhyd** exhibit D-U and U-U hydrogen bonding.

Periodic plane-wave DFT calculations with dispersion corrections were performed on both crystal structures. These simulations confirmed that the fundamental building block for the assembly of **D-U hyd** and **D-U anhyd** is the formation of Watson-Crick (W-C) D-U dimers (Table S2), estimated to be around 18 to 20 kcal/mol (in excellent agreement with benchmark quantum-chemical calculations available in the literature[76]). W-C hydrogen bonding is particularly strong in **D-U anhyd** with N$\cdots$N distances as short as 2.67 Å and corresponding interaction energies larger than 20 kcal/mol as taken from periodic

DFT relaxed structures. In both **D-U hyd** and **D-U anhyd**, we observe the formation of doubly hydrogen bonded D:U structure (intra-layer), especially strong in the hydrated form (shortest N$\cdots$N distance approaching 2.74 Å). Layer-to-layer interactions, are typically minor and translate into D:D and U:U π-stacking (**D-U anhyd** and **D-U hyd** with a degree of parallel displacement) and also D:U (**D-U hyd** only). According to periodic DFT, such interactions are typically amounting to $\sim$ 30 to 50 % energy of the corresponding (intra-layer) hydrogen-bonded ones. Formation energies obtained by periodic DFT constraining experimental cells are estimated to be -7.1 kcal/mol for **D-U hyd** and +2.2 kcal/mol for **D-U anhyd**, confirming the stability of hydrated form due to the role of water in forming inter-layer hydrogen bonds. Besides, in **D-U anhyd** we observe small distortions from co-planarity. More details on calculation parameters and related analysis can be found in the Experimental Section as well as Table S1 and S2.

Next, we aimed to study the fate of D-U base pairs under the scenario that could mimic UV irradiation on an early Earth. We investigated the supramolecular arrangement of **D-U hyd** in an aqueous solution and the sensitivity to UV light with respect to its components. We have performed a series of UVRR measurements using 266 nm as excitation wavelength and *in operando* conditions. Indeed, in our experiment, the aqueous solutions of D, U, and **D-U hyd** were irradiated with UV light (about 40 mW/cm^{-1}), and the resonance Raman spectrum was simultaneously collected from the same scattering volume as a function of the irradiation time. Although both D and U were already investigated in the context of UVRR,[77,78] the related photodegradation aspects were not addressed. Besides, while small effects are expected from purine bases, in nucleobases such as U, the formation of CPD in specific conditions is a general and established photochemical mechanism that has been widely explored in experiments[79–81] and simulations.[82–86]

Interestingly, our results point to negligible effects observed in pure U aqueous solutions (Figure S20). On the other hand, for D (Figure S21) and especially **D-U hyd** (Figure 4) aqueous solutions at 288 K, we observed a systematic decrease of the signal that we possibly

relate to a photodegradation pathway.[87] Samples were prepared from crystalline compounds dissolved in pure water, with concentrations around 3-6 $\cdot 10^{-4}$ M providing good scattering profiles. We performed a set of 24 measurements at 288 K, each obtained by collecting UVRR signal for 10' (minutes) of exposition time and found that **D-U hyd** showed a decrease in scattering intensities in practically all vibrational peaks (Figure 4). We have focused on a few wavenumber intervals and fit the time traces with monoexponential decay profiles of the kind $I = I_0 \exp(-bt)$ that reproduced the experimental trends reasonably well. It appears that U components in **D-U hyd** feature a slightly faster decay, and in general, the **D-U hyd** signal decays faster than for pure D (see Table S4 for fit details). At 266 nm, the system showing the most intense scattering is U, probably due to the best match with resonance conditions. Possibly due to this reason, vibrations that could be attributed to U components also dominate in intensity for **D-U hyd** spectra (see Table S3 for a list of attributions). Purine nucleobases, especially in the absence of sugar, have been generally considered quite resistant to UV light.[88,89] Recently, Caldero-Rodriguez *et al.*[90] have been investigating D photochemistry and photophysics, concluding that its behavior follows a fast non-radiative deactivation and/or a weak fluorescence essentially, while only 2% of D degrades under 287 nm light. Our results show that D is less resistant than expected. On the other hand, we expected U to manifest a photoreactive tendency, but we only observed this in the D-U assemblies. It is also important to stress that there is no consensus about the results of the photodimerization reactions obtained by many groups through the years.[80] It appears that even when considering the same environment (e.g. fluid aqueous solutions), there are disagreements on the yields and the proportions of the different photoproducts - suggesting these processes are all strongly dependent on a set of experimental conditions. Interestingly, Yarasi *et al.* concluded that U was less prone to thymine in populating the mode that is connected to such photoreactive path.[78] Discussing the early-stage excited-state dynamics inferred from resonant Raman measurements, the authors suggested that in thymine, the presence of a methyl substituent would cause vibrational-electronic coupled

motion to be more localized and more prone to undergo photochemistry at C5-C6 levels.

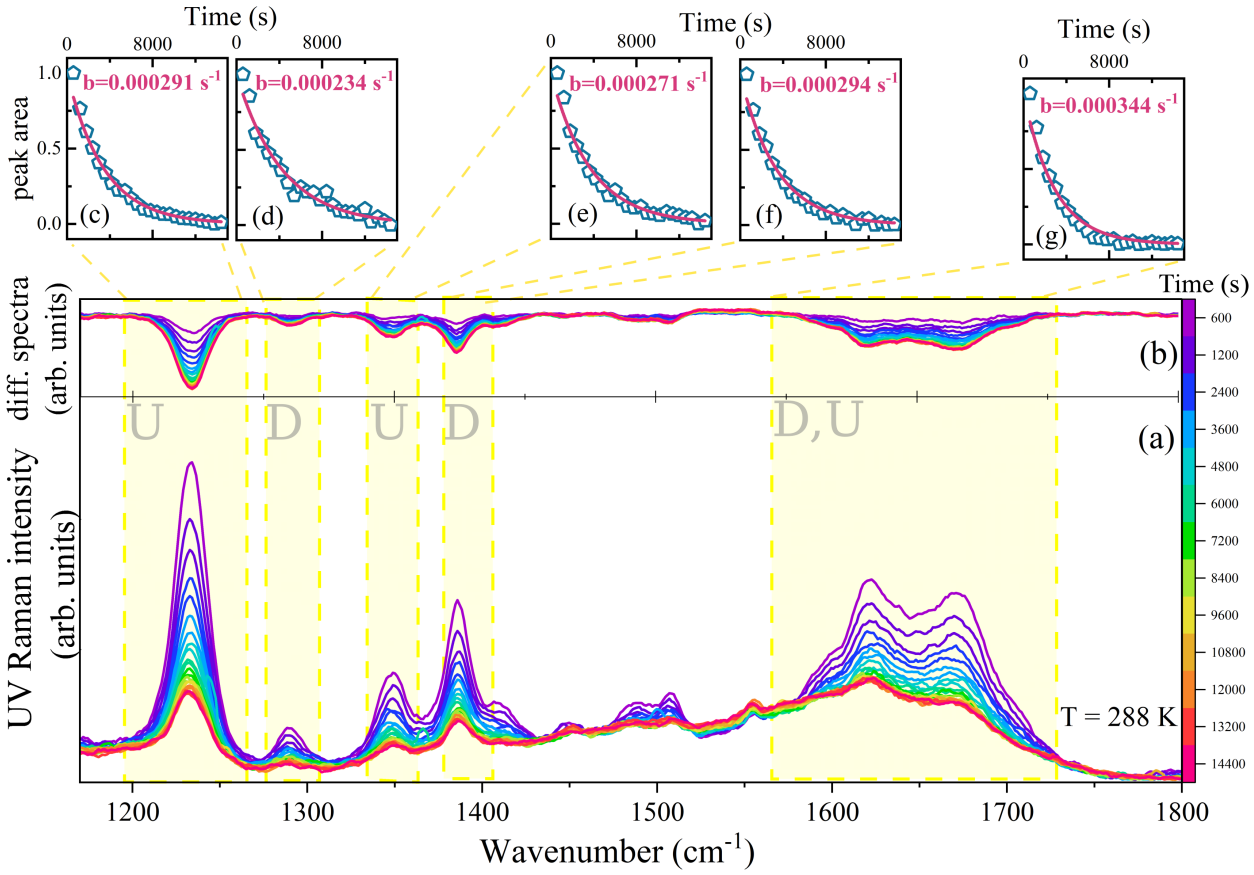

Figure 4: Effect of UV irradiation directly measured via UV resonance Raman spectroscopy at 266 nm for D-U aqueous solution, collecting one spectrum each 10' of exposure time (time is traced by the color scale on the right side) at 288 K. Upper insets: time traces and monoexponential fitting coefficient of spectral regions highlighted in yellow. Details are provided in Tables S3 and S4.

To understand the effects of D-U base-pairing on the photodestruction of U, we analyze both U and D-U potential energy surfaces in the ground and excited state. As a photoreactive path, we are here focusing on the cyclodimerization (formation of CPD). We will not discuss the U photohydration reaction, as this is known to be reversible and with negligible yields at pH $> \sim 6$, nor other less relevant addictions.[81] A combination of two coordinates is known to be relevant for the formation of U CPDs, namely the one involving C5 and C6 intra-stack coordinates. We have decided to approach our computational investigation by probing the shape of the potential energy surface with respect to these two coordinates as

well as searching possible conical intersections (CI), typically involved in such photochemical pathways. We only focus here on the *face-to-face* arrangements of uracil dimers since it has been recently suggested to be the largely dominating photoreactive reactive channel for CPD.[85] We have defined two coordinates d(C5C6') and d(C6C5'), shortly dCC1 and dCC2, respectively. We have built potential energy surfaces (PESs) in a vacuum, for both the case of two U stacking (UU) and two U stacking with a D forming hydrogen bonds with one of the U molecules (D:UU) - as inspired by the **D-U anhyd** crystal structure. Such constructed ground state DFT relaxed PES at DFT-ωB97XD level of theory, as well as relaxed S_1 TD-DFT relaxed PES (same functional) are reported in Figure 5b and Figure 5d. In such systems, the photoreactive potential energy surfaces feature a CI, which presence in CPDs has been demonstrated in multiple flavors.[84,85,91] For both our model systems, we have also performed CASSCF calculations and found that the CI is still encountered regardless of the presence of D. The location of the CIs is also included in Figure 5. DFT calculations, although inaccurate in describing CI region, can describe the PES shapes and qualitatively point to the regions where the CI is located. The PESs clearly feature the covalent cyclodimer and the stacked dimer as two low-energy basins. Interestingly, in our S_1 relaxed PESs, we found a small barrier from the cyclodimer to the region of the CIs. The presence of D obviously de-symmetrizes the surface and the location of the CI. The main consequence of the hydrogen-bonded D is the possibility of accepting a further hydrogen bond with the U-sandwiched molecules (as shown in Figure 5a). Although these results are in-vacuum, they still suggest how D could effectively promote U photodimerization by forming hydrogen bonds with two U molecules simultaneously. We speculate that this could dynamically translate into longer-living non-covalent structures in the presence of D, hence increasing the probability of photodimerization. Interestingly, while we limited our analysis to singlet states, we found that for given U:U configurations, an intermolecular proton transfer may take place (see Figure 5d). However this may not be a stable configuration (see SI Figure S25). Exploring all possible photochemical pathways in a complex system, such as D-U

self-assembly in aqueous solutions, and studying the most relevant structural configurations that would occur by sampling is beyond the scope of the current work.

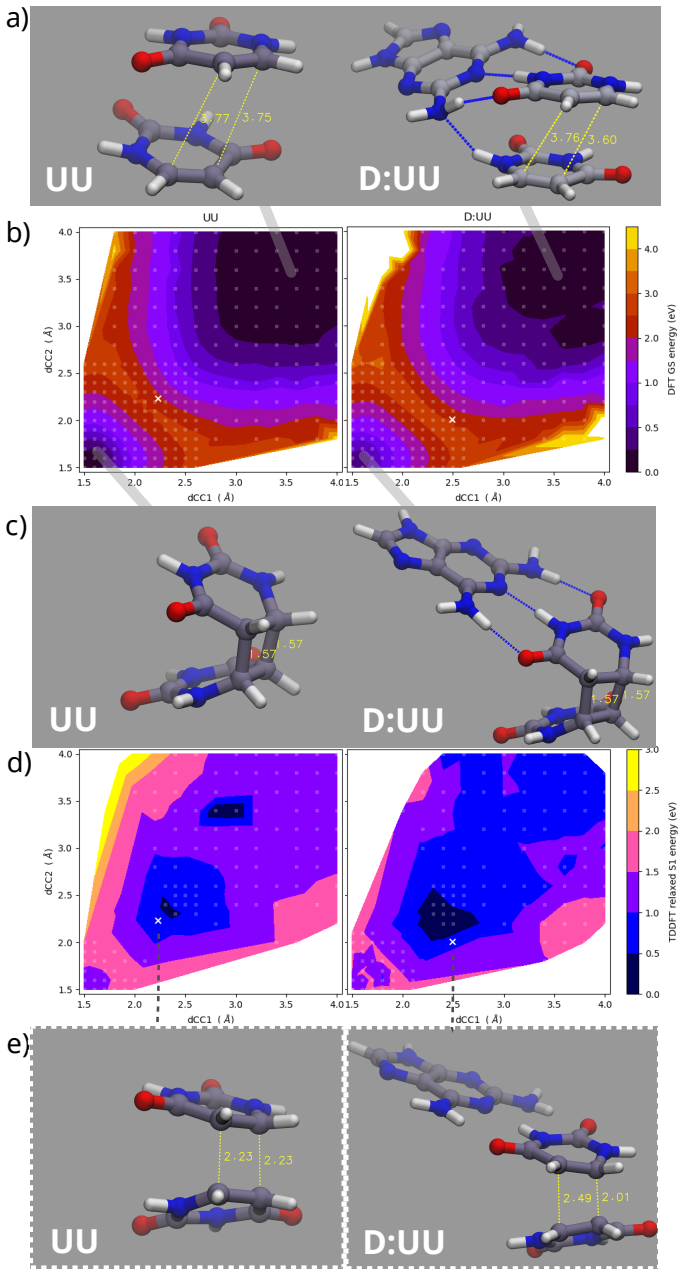

Figure 5: a) UU and D:UU π-stacking dimer and c) UU covalent CPD and D:UU covalent CPD structures obtained as ground state minima ωB97XD DFT (details in Table S5). dCC1 and dCC2 are shown in yellow. b) Ground state ωB97XD DFT potential energy constructed as relaxed scan along two relevant CC coordinates: dCC1, dCC2 (the grid of evaluated points is shaded). The region where the CI (at CASSCF) were found are marked with a white cross. d) Relaxed first excited state ωB97XD DFT PES inferred from the points that successfully converged (marked in shaded grey). The minima for UU potential in the region of dCC1, dCC2 = $\sim$(3.0,3.5) corresponds to a transfer of a proton to the oxygen of the nearby U molecule (see SI Fig. S25). The region where the CI were found are marked with a white cross. e) Structures identified at the conical intersections via CASSCF, with dCC1 and dCC2 corresponding values marked in yellow.

Conclusion

So far, the complementary base-pairing of free canonical nucleobases like U, under the prebiotic conditions, was only hypothesized. However, our results, which include *in situ* synchrotron PXRD monitoring, show that canonical U base pairs with non-canonical D under the reaction conditions of different water availability and temperatures. Some reaction conditions compatible with D-U base-pairing might have been available on early Earth or extraterrestrial bodies, for example, by wet/dry cycling in hydrothermal land-based pools or under extraterrestrial conditions of meteorite alteration events. We solved the crystal structures of the resulting hydrated and hydrated D-U base-paired cocrystal assemblies from SCXRD and 3D ED data. Furthermore, we have found experimentally by *in situ* UVRR spectroscopy that D-U aqueous solutions undergo photochemical degradation under 266 nm light, while pure U aqueous solutions do not. Our quantum-chemical and DFT simulations suggest that this may be due to the ability of D to form hydrogen bonds to two U molecules in a π-stacking configuration - hence promoting the photoreaction to CPDs. Our combined state-of-the-art experimental and theoretical studies confirm how the stability of canonical nucleobases depends on many environmental factors and how base-pairing of free nucleobases may affect their photostability.

The propensity for covalent bond formation is primarily a criterion for judging whether a compound or reaction pathway is plausibly prebiotic. We propose that non-covalent interactions between small building blocks of life may provide new insights into chemical evolution. In particular, intermolecular interactions between nucleobases can significantly alter their (already complex) potential energy landscapes and dynamically opens the possibility to photoactivation-driven reactions. Thus, in the early stages of chemical evolution, nucleobases with complementary supramolecular interactions may have been selected or neglected based on their thermodynamic and kinetic stability or photostability.[12,28]

Acknowledgement

T.S. thanks Dr. J. Dworkin (NASA), Prof. M. P. Callahan (Boise), Prof. J. G. Hernández (UdeA), and Dr. S. Lukin (SeaCras) for the discussion. We acknowledge DESY (Hamburg, Germany), a member of the Helmholtz Association HGF, for the provision of experimental facilities. Parts of this research were carried out at PETRA III, beamline P02.1. Beamtime was allocated for proposal I-20220019 EC. L.G. and T.S. acknowledge the CERIC-ERIC Consortium for the access to experimental facilities (proposals 20212028, 20212125, and 20222150). K.U. acknowledges Croatian Science Foundation (grant no. IP-2020-02-4702) for financial support. L.G. acknowledges the Croatian Science Foundation (HrZZ), via the project IP-2020-02-7262 (HYMO4EXNOMOMA). A.K. and G.M. acknowledge the financial support from the Slovenian Research Agency (research core funding no. P1-0021).

Supporting Information Available

References

(1) Watson, J. D.; Crick, F. H. C. Genetical Implications of the Structure of Deoxyribonucleic Acid. *Nature* **1953**, *171*, 964–967.

(2) Schuster, G. B.; Cafferty, B. J.; Karunakaran, S. C.; Hud, N. V. Water-Soluble Supramolecular Polymers of Paired and Stacked Heterocycles: Assembly, Structure, Properties, and a Possible Path to Pre-RNA. *J. Am. Chem. Soc.* **2021**, *143*, 9279–9296.

(3) Ts'o, P. O. P.; Melvin, I. S.; Olson, A. C. Interaction and Association of Bases and Nucleosides in Aqueous Solutions. *J. Am. Chem. Soc.* **1963**, *85*, 1289–1296.

(4) Ts'o, P. O. P. Chapter "Bases, nucleosides, and nucleotides" in "Basic Principles in Nucleic Acid Chemistry". *New York: Academic Press* **1974**, *I*, 453–584.

(5) Cieplak, P.; Kollman, P. A. Calculation of the free energy of association of nucleic acid bases in vacuo and water solution. *J. Am. Chem. Soc.* **1988**, *110*, 3734–3739.

(6) Stolar, T.; Lukin, S.; Etter, M.; Rajić Linarić, M.; Užarević, K.; Meštrović, E.; Halasz, I. DNA-specific selectivity in pairing of model nucleobases in the solid state. *Chem. Commun.* **2020**, *56*, 13524–13527.

(7) Hud, N.; Jain, S.; Li, X.; Lynn, D. Addressing the Problems of Base Pairing and Strand Cyclization in Template-Directed Synthesis. *Chem. Biodivers.* **2007**, *4*, 768–783.

(8) Saladino, R.; Crestini, C.; Ciciriello, F.; Costanzo, G.; Di Mauro, E. Formamide Chemistry and the Origin of Informational Polymers. *Chem. Biodivers.* **2007**, *4*, 694–720.

(9) Krishnamurthy, R. Role of pKa of Nucleobases in the Origins of Chemical Evolution. *Acc. Chem. Res.* **2012**, *45*, 2035–2044.

(10) Menor-Salván, C.; Marín-Yaseli, M. R. Prebiotic chemistry in eutectic solutions at the water–ice matrix. *Chem. Soc. Rev.* **2012**, *41*, 5404–5415.

(11) Rios, A. C.; Tor, Y. On the Origin of the Canonical Nucleobases: An Assessment of Selection Pressures across Chemical and Early Biological Evolution. *Isr. J. Chem.* **2013**, *53*, 1–15.

(12) Fialho, D. M.; Roche, T. P.; Hud, N. V. Prebiotic Syntheses of Noncanonical Nucleosides and Nucleotides. *Chem. Rev.* **2020**, *120*, 4806–4830.

(13) Joyce, G. F.; Schwartz, A. W.; Miller, S. L.; Orgel, L. E. The case for an ancestral genetic system involving simple analogues of the nucleotides. *Proc. Natl. Acad. Sci. U.S.A.* **1987**, *84*, 4398–4402.

(14) Cafferty, B. J.; Fialho, D. M.; Khanam, J.; Krishnamurthy, R.; Hud, N. V. Spontaneous formation and base pairing of plausible prebiotic nucleotides in water. *Nat Commun* **2016**, *7*, 11328.

(15) Yadav, M.; Kumar, R.; Krishnamurthy, R. Chemistry of Abiotic Nucleotide Synthesis. *Chem. Rev.* **2020**, *120*, 4766–4805.

(16) Islam, S.; Powner, M. W. Prebiotic Systems Chemistry: Complexity Overcoming Clutter. *Chem* **2017**, *2*, 470–501.

(17) Powner, M. W.; Gerland, B.; Sutherland, J. D. Synthesis of activated pyrimidine ribonucleotides in prebiotically plausible conditions. *Nature* **2009**, *459*, 239–242.

(18) Becker, S.; Feldmann, J.; Wiedemann, S.; Okamura, H.; Schneider, C.; Iwan, K.; Crisp, A.; Rossa, M.; Amatov, T.; Carell, T. Unified prebiotically plausible synthesis of pyrimidine and purine RNA ribonucleotides. *Science* **2019**, *366*, 76–82.

(19) Callahan, M. P.; Smith, K. E.; Cleaves, H. J.; Ruzicka, J.; Stern, J. C.; Glavin, D. P.; House, C. H.; Dworkin, J. P. Carbonaceous meteorites contain a wide range of extraterrestrial nucleobases. *Proc. Natl. Acad. Sci. U.S.A.* **2011**, *108*, 13995–13998.

(20) Oba, Y.; Takano, Y.; Furukawa, Y.; Koga, T.; Glavin, D. P.; Dworkin, J. P.; Naraoka, H. Identifying the wide diversity of extraterrestrial purine and pyrimidine nucleobases in carbonaceous meteorites. *Nat Commun* **2022**, *13*, 2008.

(21) Szabla, R.; Zdrowowicz, M.; Spisz, P.; Green, N. J.; Stadlbauer, P.; Kruse, H.; Šponer, J.; Rak, J. 2,6-diaminopurine promotes repair of DNA lesions under prebiotic conditions. *Nature Communications* **2021**, *12*, 3018.

(22) Jiménez, E. I.; Gibard, C.; Krishnamurthy, R. Prebiotic Phosphorylation and Concomitant Oligomerization of Deoxynucleosides to form DNA. *Angew. Chem. Int. Ed.* **2021**, *60*, 10775–10783.

(23) Kirnos, M. D.; Khudyakov, I. Y.; Alexandrushkina, N. I.; Vanyushin, B. F. 2-aminoadenine is an adenine substituting for a base in S-2L cynophage DNA. *Nature* **1977**, *270*, 369–370.

(24) Khudyakov, I. Y.; Kirnos, M. D.; Alexandrushkina, N. I.; Vanyushin, B. F. Cyanophage S-2L Contains DNA With 2,6-Diaminopurine Substituted for Adenine. *Virology* **1978**, *18*, 8–18.

(25) Pezo, V.; Jaziri, F.; Bourguignon, P.-Y.; Louis, D.; Jacobs-Sera, D.; Rozenski, J.; Pochet, S.; Herdewijn, P.; Hatfull, G. F.; Kaminski, P.-A.; Marliere, P. Noncanonical DNA polymerization by aminoadenine-based siphoviruses. *Science* **2021**, *372*, 520–524.

(26) Sleiman, D.; Garcia, P. S.; Lagune, M.; Loc'h, J.; Haouz, A.; Taib, N.; Röthlisberger, P.; Gribaldo, S.; Marlière, P.; Kaminski, P. A. A third purine biosynthetic pathway encoded by aminoadenine-based viral DNA genomes. *Science* **2021**, *372*, 516–520.

(27) Zhou, Y.; Xu, X.; Wei, Y.; Cheng, Y.; Guo, Y.; Khudyakov, I.; Liu, F.; He, P.; Song, Z.; Li, Z.; Gao, Y.; Ang, E. L.; Zhao, H.; Zhang, Y.; Zhao, S. A widespread pathway for substitution of adenine by diaminopurine in phage genomes. *Science* **2021**, *372*, 512–516.

(28) Boldissar, S.; de Vries, M. S. How nature covers its bases. *Phys. Chem. Chem. Phys.* **2018**, *20*, 9701–9716.

(29) Green, N. J.; Xu, J.; Sutherland, J. D. Illuminating Life's Origins: UV Photochemistry in Abiotic Synthesis of Biomolecules. *J. Am. Chem. Soc.* **2021**, *143*, 7219–7236.

(30) Milovanović, B.; Novak, J.; Etinski, M.; Domcke, W.; Došlić, N. Simulation of UV absorption spectra and relaxation dynamics of uracil and uracil–water clusters. *Phys. Chem. Chem. Phys.* **2021**, *23*, 2594–2604.

(31) Gustavsson, T.; Bányász, ; Lazzarotto, E.; Markovitsi, D.; Scalmani, G.; Frisch, M. J.; Barone, V.; Improta, R. Singlet Excited-State Behavior of Uracil and Thymine in Aqueous Solution: A Combined Experimental and Computational Study of 11 Uracil Derivatives. *J. Am. Chem. Soc.* **2006**, *128*, 607–619.

(32) Beckstead, A. A.; Zhang, Y.; de Vries, M. S.; Kohler, B. Life in the light: nucleic acid photoproperties as a legacy of chemical evolution. *Phys. Chem. Chem. Phys.* **2016**, *18*, 24228–24238.

(33) Rietveld, H. M. A profile refinement method for nuclear and magnetic structures. *J. Appl. Crystallogr.* **1969**, *2*, 65–71.

(34) TOPAS (version 4.2), Bruker-AXS: Karlsruhe, Germany, 2009.

(35) CrysAlis^{PRO}, Rigaku Oxford Diffraction, 2018, version: 1.171.39.46, Rigaku Corporation, Oxford, UK.

(36) Sheldrick, G. M. *SHELXT* – Integrated space-group and crystal-structure determination. *Acta Crystallogr. A* **2015**, *71*, 3–8.

(37) Spek, A. L. Structure validation in chemical crystallography. *Acta Crystallogr. D* **2009**, *65*, 148–155.

(38) Farrugia, L. J. *ORTEP*-3 for Windows - a version of *ORTEP*-III with a Graphical User Interface (GUI). *J. Appl. Crystallogr.* **1997**, *30*, 565.

(39) Macrae, C. F.; Sovago, I.; Cottrell, S. J.; Galek, P. T. A.; McCabe, P.; Pidcock, E.; Platings, M.; Shields, G. P.; Stevens, J. S.; Towler, M.; Wood, P. A. *Mercury 4.0*: from visualization to analysis, design and prediction. *J. Appl. Crystallogr.* **2020**, *53*, 226–235.

(40) Ito, S.; White, F. J.; Okunishi, E.; Aoyama, Y.; Yamano, A.; Sato, H.; Ferrara, J. D.; Jasnowski, M.; Meyer, M. Structure determination of small molecule compounds by an electron diffractometer for 3D ED/MicroED. *CrystEngComm* **2021**, *23*, 8622–8630.

(41) Rigaku Oxford Diffraction, CrysAlis^{PRO} software system, Rigaku Corporation, Wrocław, Poland, 2023 (version 1.171.43.53a).

(42) Sheldrick, G. M. Crystal structure refinement with *SHELXL*. *Acta Crystallogr. C* **2015**, *71*, 3–8.

(43) Rigaku Oxford Diffraction, AutoChem 6 software system in conjunction with OLEX2, Rigaku Corporation, Wrocław, Poland, 2023 (version 1.5-ac6-009).

(44) Dolomanov, O. V.; Bourhis, L. J.; Gildea, R. J.; Howard, J. A. K.; Puschmann, H. *OLEX2*: a complete structure solution, refinement and analysis program. *J. Appl. Crystallogr.* **2009**, *42*, 339–341.

(45) Thorn, A.; Dittrich, B.; Sheldrick, G. M. Enhanced rigid-bond restraints. *Acta Crystallogr. A* **2012**, *68*, 448–451.

(46) Giannozzi, P. et al. QUANTUM ESPRESSO: a modular and open-source software project for quantum simulations of materials. *J. Phys. Condens. Matter* **2009**, *21*, 395502.

(47) Giannozzi, P. et al. Advanced capabilities for materials modelling with Quantum ESPRESSO. *J. Phys. Condens. Matter* **2017**, *29*, 465901.

(48) Garrity, K. F.; Bennett, J. W.; Rabe, K. M.; Vanderbilt, D. Pseudopotentials for high-throughput DFT calculations. *Comput. Mater. Sci* **2014**, *81*, 446–452.

(49) Berland, K.; Hyldgaard, P. Exchange functional that tests the robustness of the plasmon description of the van der Waals density functional. *Phys. Rev. B* **2014**, *89*, 035412.

(50) Berland, K.; Arter, C. A.; Cooper, V. R.; Lee, K.; Lundqvist, B. I.; Schröder, E.; Thonhauser, T.; Hyldgaard, P. van der Waals density functionals built upon the electron-gas tradition: Facing the challenge of competing interactions. *J. Chem. Phys.* **2014**, *140*, 18A539.

(51) Brown-Altvater, F.; Rangel, T.; Neaton, J. B. Ab initio phonon dispersion in crystalline naphthalene using van der Waals density functionals. *Phys. Rev. B* **2016**, *93*, 195206.

(52) Rangel, T.; Berland, K.; Sharifzadeh, S.; Brown-Altvater, F.; Lee, K.; Hyldgaard, P.; Kronik, L.; Neaton, J. B. Structural and excited-state properties of oligoacene crystals from first principles. *Phys. Rev. B* **2016**, *93*, 115206.

(53) Lončarić, I.; Popović, J.; Despoja, V.; Burazer, S.; Grgičević, I.; Popović, D.; Skoko, Ž. Reversible Thermosalient Effect of N′-2-Propylidene-4-hydroxybenzohydrazide Accompanied by an Immense Negative Compressibility: Structural and Theoretical Arguments Aiming toward the Elucidation of Jumping Phenomenon. *Cryst. Growth Des* **2017**, *17*, 4445–4453.

(54) Hyldgaard, P.; Jiao, Y.; Shukla, V. Screening nature of the van der Waals density functional method: a review and analysis of the many-body physics foundation. *J. Phys. Condens. Matter* **2020**, *32*, 393001.

(55) Rossi, B.; Bottari, C.; Catalini, S.; D'Amico, F.; Gessini, A.; Masciovecchio, C. In *Molecular and Laser Spectroscopy*; Gupta, V., Ozaki, Y., Eds.; Elsevier, 2020; pp 447–482.

(56) Frisch, M. J.; Trucks, G. W.; Schlegel, H. B.; Scuseria, G. E.; Robb, M. A.; Cheeseman, J. R.; Scalmani, G.; Barone, V.; Petersson, G. A.; Nakatsuji, H.; et al., 2009; *Gaussian 09*, Revision E.01; Gaussian, Inc.: Wallingford, CT, 2009.

(57) Chai, J.-D.; Head-Gordon, M. Long-range corrected hybrid density functionals with damped atom–atom dispersion corrections. *Phys. Chem. Chem. Phys.* **2008**, *10*, 6615–6620.

(58) Hariharan, P. C.; Pople, J. A. The influence of polarization functions on molecular orbital hydrogenation energies. *Theoret. Chim. Acta* **1973**, *28*, 213–222.

(59) Frisch, M. J. et al. Gaussian˜16 Revision C.01. 2016; Gaussian Inc. Wallingford CT.

(60) Huskić, I.; Lennox, C. B.; Friščić, T. Accelerated ageing reactions: towards simpler, solvent-free, low energy chemistry. *Green Chem.* **2020**, *22*, 5881–5901.

(61) Bolm, C.; Mocci, R.; Schumacher, C.; Turberg, M.; Puccetti, F.; Hernandez, J. G. Mechanochemical Activation of Iron Cyano Complexes : A Prebiotic Impact Scenario for the Synthesis of a-Amino Acid Derivatives. *Angew. Chem. Int. Ed.* **2018**, *57*, 2423–2426.

(62) Lamour, S.; Pallmann, S.; Haas, M.; Trapp, O. Prebiotic Sugar Formation Under Non-aqueous Conditions and Mechanochemical Acceleration. *Life* **2019**, *9*, 52.

(63) Haas, M.; Lamour, S.; Christ, S. B.; Trapp, O. Mineral-mediated carbohydrate synthesis by mechanical forces in a primordial geochemical setting. *Commun Chem* **2020**, *3*, 140.

(64) Elsila, J. E.; Johnson, N. M.; Glavin, D. P.; Aponte, J. C.; Dworkin, J. P. Amino acid abundances and compositions in iron and stony-iron meteorites. *Meteorit Planet Sci* **2021**, *56*, 586–600.

(65) Stolar, T.; Grubešić, S.; Cindro, N.; Meštrović, E.; Užarević, K.; Hernández, J. G. Mechanochemical Prebiotic Peptide Bond Formation. *Angew. Chem. Int. Ed.* **2021**, *60*, 12727–12731.

(66) Damer, B.; Deamer, D. The Hot Spring Hypothesis for an Origin of Life. *Astrobiology* **2020**, *20*, 429–452.

(67) Atria, A. M.; Garland, M. T.; Baggio, R. 2,6-Diamino-9*H*-purine monohydrate and bis-(2,6-diamino-9*H*-purin-1-ium) 2-(2-carboxylatophenyl)acetate heptahydrate: two simple structures with very complex hydrogen-bonding schemes. *Acta Crystallogr. C* **2010**, *66*, o547–o552.

(68) Stolar, T.; Alić, J.; Lončarić, I.; Etter, M.; Jung, D.; Farha, O. K.; Đilović, I.; Meštrović, E.; Užarević, K. Sustainable solid form screening: mechanochemical control over

nucleobase hydrogen-bonded organic framework polymorphism. *CrystEngComm* **2022**, *24*, 6505–6511.

(69) Orgel, L. E. Prebiotic Chemistry and the Origin of the RNA World. *Crit. Rev. Biochem. Mol. Biol.* **2004**, *39*, 99–123.

(70) Müller, U. F.; Elsila, J.; Trail, D.; DasGupta, S.; Giese, C.-C.; Walton, C. R.; Cohen, Z. R.; Stolar, T.; Krishnamurthy, R.; Lyons, T. W.; Rogers, K. L.; Williams, L. D. Prebiotic Chemistry and the Origin of the RNA World. *Orig Life Evol Biosph* **2022**, *52*, 165–181.

(71) Van Kranendonk, M. J.; Baumgartner, R.; Djokic, T.; Ota, T.; Steller, L.; Garbe, U.; Nakamura, E. Elements for the Origin of Life on Land: A Deep-Time Perspective from the Pilbara Craton of Western Australia. *Astrobiology* **2021**, *21*, 39–59.

(72) Pearce, B. K. D.; Pudritz, R. E.; Semenov, D. A.; Henning, T. K. Origin of the RNA world: The fate of nucleobases in warm little ponds. *Proc. Natl. Acad. Sci. U.S.A.* **2017**, *114*, 11327–11332.

(73) Brearley, A. J. The Action of Water. *Meteor. Early Solar Syst. II* **2006**, 587–624.

(74) Hamilton, V. E.; Goodrich, C. A.; Treiman, A. H.; Connolly, H. C.; Zolensky, M. E.; Shaddad, M. H. Meteoritic evidence for a Ceres-sized water-rich carbonaceous chondrite parent asteroid. *Nat Astron* **2020**,

(75) Oba, Y. et al. Uracil in the carbonaceous asteroid (162173) Ryugu. *Nat Commun* **2023**, *14*, 1292.

(76) Šponer, J.; Jurečka, P.; Hobza, P. Accurate Interaction Energies of Hydrogen-Bonded Nucleic Acid Base Pairs. *J. Am. Chem. Soc.* **2004**, *126*, 10142–10151.

(77) Dhaouadi, Z.; Ghomi, M.; Mojzes, P.; Turpin, P. Y.; Chinsky, L. Vibrational mode

analysis of 2-aminoadenine and its deuterated species from Raman and ultraviolet resonance Raman data. *Eur. Biophys. J.* **1994**, *23*, 95–104.

(78) Yarasi, S.; Ng, S.; Loppnow, G. R. Initial Excited-State Structural Dynamics of Uracil from Resonance Raman Spectroscopy Are Different from Those of Thymine (5-Methyluracil). *J. Phys. Chem. B* **2009**, *113*, 14336–14342.

(79) Varghese, A. J. Photochemistry of uracil and uridine. *Biochem* **1971**, *10*, 4283–4290.

(80) Shetlar, M. D.; Basus, V. J. The Photochemistry of Uracil: A Reinvestigation. *Photochemistry and Photobiology* **2011**, *87*, 82–102.

(81) Fisher, G.; Johns, H. *Photochemistry and Photobiology of Nucleic Acids*; 1976; Vol. 1; pp 225–294.

(82) González-Ramírez, I.; Roca-Sanjuán, D.; Climent, T.; Serrano-Pérez, J. J.; Merchán, M.; Serrano-Andrés, L. On the photoproduction of DNA/RNA cyclobutane pyrimidine dimers. *Theor. Chem. Acc.* **2011**, *128*, 705–711.

(83) Giussani, A.; Conti, I.; Nenov, A.; Garavelli, M. Photoinduced formation mechanism of the thymine–thymine (6–4) adduct in DNA; a QM (CASPT2//CASSCF): MM (AMBER) study. *Faraday Discuss.* **2018**, *207*, 375–387.

(84) Delchev, V. B.; Domcke, W. Ab initio study of the cyclodimerization of uracil through butane-like and oxetane-like conical intersections. *J. Photochem. Photobiol. A* **2013**, *271*, 1–7.

(85) Milovanović, B.; Novak, J.; Etinski, M.; Domcke, W.; Došlić, N. On the propensity of formation of cyclobutane dimers in face-to-face and face-to-back uracil stacks in solution. *Phys. Chem. Chem. Phys.* **2022**, *24*, 14836–14845.

(86) Martinez Fernandez, L.; Santoro, F.; Improta, R. Nucleic Acids as a Playground for the

Computational Study of the Photophysics and Photochemistry of Multichromophore Assemblies. *Acc. Chem. Res.* **2022**, *55*, 2077–2087.

(87) Winkler, M.; Giuliano, B. M.; Caselli, P. UV Resistance of Nucleosides—An Experimental Approach. *ACS Earth Space Chem.* **2020**, *4*, 2320–2326.

(88) Davies, R. J. H. Ultraviolet Radiation Damage in DNA. *Biochem. Soc. Trans.* **1995**, *23*, 407–418.

(89) Poch, O.; Jaber, M.; Stalport, F.; Nowak, S.; Georgelin, T.; Lambert, J.-F.; Szopa, C.; Coll, P. Effect of Nontronite Smectite Clay on the Chemical Evolution of Several Organic Molecules under Simulated Martian Surface Ultraviolet Radiation Conditions. *Astrobiology* **2015**, *15*, 221–237.

(90) Caldero-Rodríguez, N. E.; Ortiz-Rodríguez, L. A.; Gonzalez, A. A.; Crespo-Hernández, C. E. Photostability of 2,6-diaminopurine and its 2-deoxyriboside investigated by femtosecond transient absorption spectroscopy. *Phys. Chem. Chem. Phys.* **2022**, *24*, 4204–4211.

(91) Kancheva, B. P.; Delchev, B. V. Comparative Study of the Gas-phase Cyclodimer Formations of Uracil and 6-azauracil in Excited State and through Conical Intersections S0/S1. *Acta Chim Slov* **2018**, *65*, 521–530.

TOC Graphic